RL-TR-97-109
Final Technical Report
October 1997

MECHANISM AND APPLICATIONS OF MICROWAVE-FREQUENCY INTENSITY OSCILLATION OF LASER DIODES WITH SHORT EXTERNAL CAVITY

Rochester Institute of Technology

Guifang Li

APPROVED FOR PUBLIC RELEASE; DISTRIBUTION UNLIMITED.

Rome Laboratory
Air Force Materiel Command
Rome, New York

This report has been reviewed by the Rome Laboratory Public Affairs Office (PA) and is releasable to the National Technical Information Service (NTIS). At NTIS it will be releasable to the general public, including foreign nations.

RL-TR-97-109 has been reviewed and is approved for publication.

APPROVED: Steven T. Jones

STEVEN T. JONES
Project Engineer

FOR THE DIRECTOR: Donald W. Hanson

DONALD W. HANSON, Director
Surveillance & Photonics Directorate

REPORT DOCUMENTATION PAGE

Form Approved
OMB No. 0704-0188

1. AGENCY USE ONLY *(Leave blank)*

2. REPORT DATE
October 1997

3. REPORT TYPE AND DATES COVERED
FINAL, Mar 96 - Mar 97

4. TITLE AND SUBTITLE
MECHANISM AND APPLICATIONS OF MICROWAVE-FREQUENCY INTENSITY OSCILLATION OF LASER DIODES WITH SHORT EXTERNAL CAVITY

5. FUNDING NUMBERS

C - F30602-96-2-0063
PE - 62702F
PR - 4600
TA - P5
WU - PH

6. AUTHOR(S)
Dr. Guifang Li

7. PERFORMING ORGANIZATION NAME(S) AND ADDRESS(ES)
Rochester Institute of Technology
75 Highpower Rd
Rochester NY 14623

8. PERFORMING ORGANIZATION REPORT NUMBER

9. SPONSORING / MONITORING AGENCY NAME(S) AND ADDRESS(ES)
Rome Laboratory/OCPC
25 Electronic Pky
Rome NY 13441-4515

10. SPONSORING / MONITORING AGENCY REPORT NUMBER

RL-TR-97-109

11. SUPPLEMENTARY NOTES

Rome Laboratory Project Engineer: Steven T. Johns, OCPC, (315) 330-4456

12a. DISTRIBUTION AVAILABILITY STATEMENT

APPROVED FOR PUBLIC RELEASE; DISTRIBUTION UNLIMITED

12b. DISTRIBUTION CODE

13. ABSTRACT *(Maximum 200 words)*
This effort investigates the mechanism and applications of microwave-frequency intensity oscillation of laser diodes with short external cavity. Future Air Force analog fiber optic links will require RF bandwidths of 10-60 GHz with dynamic range greater than 120 dB. Systems are investigated here which could deliver these specifications in a compact, light weight and low power approach. A theoretical simulation is presented using a nonlinear dynamic point of view. Analyses show that Hopf bifurcation is responsible for the occurrence of the high-frequency intensity oscillations that can be used for communication links. An experimental investigation into frequency deviation, amplitude fluctuations and phase noise was also conducted.

14. SUBJECT TERMS
microwave oscillations, laser diode, short external cavity, analog optical links

15. NUMBER OF PAGES
28

16. PRICE CODE

17. SECURITY CLASSIFICATION OF REPORT	18. SECURITY CLASSIFICATION OF THIS PAGE	19. SECURITY CLASSIFICATION OF ABSTRACT	20. LIMITATION OF ABSTRACT
UNCLASSIFIED	**UNCLASSIFIED**	**UNCLASSIFIED**	**UNLIMITED**

NSN 7540-01-280-5500

Standard Form 298 (Rev. 2-89)
Prescribed by ANSI Std. Z39-18
298-102

TABLE OF CONTENTS

LIST OF FIGURES

1. Introduction

Future military analog fiber-optic links require high-bandwidth (20-30 GHz) and large dynamic range (>120 dB) that are, furthermore, compact, light weight, and with low power consumption. Technologies that have been investigated so far can not meet the above-mentioned demands. These technologies include, cw laser diode direct modulation, mode-locked laser diode external modulation, and external modulation.

Optical coupling of a Laser diode (LD) with an external cavity (EC), such as shown schematically in Fig. 1, has been used to improve laser frequency stability and to narrow laser linewidth. Such coupling can also significantly change LD dynamics. For long (>1 cm) external cavity LDs these changes lead to chaotic self-modulation of laser light with dramatic broadening of laser spectrum ("coherence-collapse" effect). For a short EC LD there exists another type of instability associated with the EC mode interactions alone [1]. The compound-cavity mode interaction inside the regime of stable CW operation lead to the generation of high frequency (>20 GHz) microwave oscillations. Such high-frequency oscillations arise, as has been conjectured [1], if the cavity losses for the main and side compound-cavity modes of the short EC LD become equal with increasing feedback. This equalization does not lead, however, to a switching of lasing to this sidemode, but instead induces a self-mode-locking regime with deep oscillations of the laser output.

We propose to use short EC LDs as tunable microwave oscillators with frequency modulation capabilities. There are two way the frequency can be modulated [2].

- It has been shown that the oscillation frequency increases with increasing feedback. Therefore, the frequency of the microwave oscillation can be modulated by the feedback
- It should be noted that the oscillation is a result of the interaction of compound-cavity mode interaction. Therefore, once the optical length of the individual cavity is changed, the oscillation is tuned.

We have previously computed the dynamics of short EC LDs, mapped out the system parameter space for microwave oscillations, and determined the frequency range of the microwave oscillations.

The ultimate research objective is to *experimentally* demonstrate the generation of tunable microwave intensity oscillations in laser diodes with short external cavity for use in analog fiber-optic links. A better understanding of the fundamental mechanism is therefore essential for progress towards employing these devices in real applications. In this report, we document enhanced understanding of the underlying physical principle for the microwave-frequency intensity modulation from a nonlinear dynamics point of view, and ways to experimentally measure the noise characteristics of the oscillations.

2. Formulation of the Problem

2.1 Rate Equation

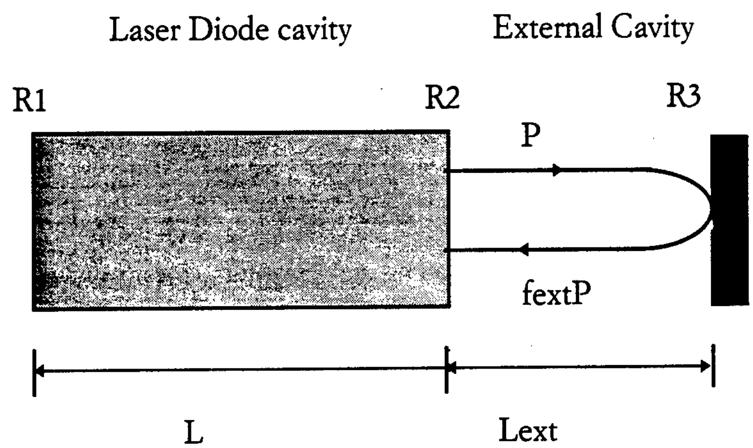

Fig. 1 Schematic of a laser diode with an external cavity.

The schematic of a semiconductor laser diode with an external cavity is shown in Fig. 1. R1 and R2 are the reflectivity of the laser facets and R3 is the reflectivity of the external mirror. L and Lext are the lengths of the laser diode cavity and the EC; fext is the feedback. We will consider $\tau\omega_R << 1$, where $\tau = 2L_{ext}/c$ is the photon round-trip time in EC and ω_R is the angular frequency of the relaxation oscillation.

We adopt the Lang and Kobayashi rate equations for the SEC LD. There are several assumptions for these rate equations. First, the solitary laser is assumed to be single mode, which implies $\tau >> \tau_0$ ($\tau_0 = 2Ln_g/c$, is the photon round-trip time in the LD-cavity, n_g is the group refraction index of the LD.). Second, $f_{ext} << 1$ which means only one round-trip of the emitted photons is significant inside the EC. Then we arrive at the following two rate equations :

$$\frac{dE(t)}{dt} = j\left[\Omega_s - \Omega + \frac{\alpha}{2} g_N (N - N_s)\right] E(t) + \frac{1}{2}(g - \frac{1}{\tau_p}) E(t) + \kappa E(t - \tau)\exp(-i\Omega\tau) \quad (1)$$

$$\frac{dN}{dt} = J - \frac{N}{\tau_{sp}} - gS \quad (2)$$

where $g = g(N)(1 - \kappa_p P)$ is the nonlinear gain where the differential gain is given by $g(N) = g_N (N - N_s)$, P is the output power, Ω_s is the resonance optical frequency of the LD without EC, α is the linewidth enhancement factor, g_N is the differential gain, τ_p is the photon lifetime in the LD cavity, τ_{sp} is the carrier lifetime due to spontaneous and nonradiative recombination, $S = |E(t)|^2$ is the photon number in the LD cavity. (output power P~S), J is the carrier injection rate. The feedback parameter is given by

$$\kappa = \frac{C_l}{\tau_0},$$

where parameter C_l which is a function of the facet and external mirror reflectivity R_2 and R_3

$$C_l = (1 - R_2)\sqrt{\frac{R_3}{R_2}}$$

is a measure of the coupling strength between the two cavities. The rate equations for the EC LD are given in equations (1) and (2). The absolute squared value of the electric field amplitude corresponds to the number of photons in the laser cavity. Equations (1) and (2) can be cast into rate equations for the photon number S, the phase ϕ , and the carrier number N:

$$\frac{dS(t)}{dt} = (g - \frac{1}{\tau_p})S(t) + 2\kappa\sqrt{S(t)}\sqrt{S(t-\tau)}\cos(\Omega_s\tau + \phi(t) - \phi(t-\tau)) \quad (3)$$

$$\frac{d\phi(t)}{dt} = \frac{\alpha}{2}g_N(N - N_s) - \kappa\frac{\sqrt{S(t-\tau)}}{\sqrt{S(t)}}\sin(\Omega_s\tau + \phi(t) - \phi(t-\tau)) \quad (4)$$

$$\frac{dN(t)}{dt} = J - \frac{N(t)}{\tau_{sp}} - gS(t) \quad (5)$$

2.2 Numerical Simulations

In numerical simulations, the system of rate equations system (3)-(5) is solved by using a fifth-order Runge-Kutta method [3],[4]. We specify the initial conditions S(0)=10, $\phi(0)=0$ and N(0)=0. In the time interval $0 \le t \le \tau$, the data of photon number S and phase ϕ are stored in memory and they are reused after the round-trip time τ of the EC in order to account for the optical feedback.

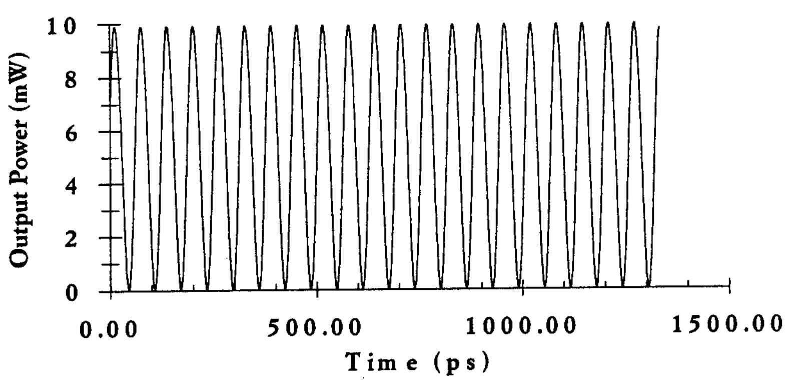

Fig. 2 The strongest oscillation for the Lext=5.25mm and the f_{ext} group. The feedback parameter is 0.206. The oscillation frequency is equal to 21.3 GHz.

2.3 An Example of High-Frequency Microwave Oscillation

For example, we set the output power P=5 mW/per facet. The calculations used the laser parameters given in Table I. Here, we also choose the EC length L_{ext} =5.25 mm. We found that the feedback parameters for the strongest modulation index occurs when f_{ext} = 0.206. Further increasing f_{ext} destroys the twin mode locking. It leads the laser operation on a new single-mode state with higher output power (7.06 mW). The strongest oscillation frequency we get in the group f_{ext} is 21.3 GHz as shown in Fig. 2.

TABLE I
List of Parameters for Fabry-Perot laser

Parameter	Symbol	Value	Units
scattering loss in the active region	α_s	3.6×10^3	m^{-1}
carrier number at transparency	N_s	2.0×10^8	
output power	P	$2.906\times10^{-8}\times S$	$mW / facet$
index of active region	n_g	4.5	
differential gain	g_N	2.2×10^3	s^{-1}
linewidth enhancement factor	α	4	
laser wavelength	λ	1.3	um
spontaneous emission lifetime	τ_s	2.0×10^{-9}	s
photon lifetime	τ_p	1.29072×10^{-12}	s
gain saturation coefficient	k_p	4.8	W^{-1}

3. Bifurcation Analysis of the ECLD

Since the problem is nonlinear in nature, there does not exist a general analytical methodology that can lead to a global conclusion of the operation characteristics of the

ECLD. Our approach is to establish a numerical technique that is capable of predicting the nature of the ECLD output given a complete set of parameters for the ECLD without numerical integration described in Section 2. We used a public-domain software called AUTO to investigate the dynamics of laser diodes with short external cavity. AUTO was developed in the Applied Mathematics Department at the California Institute of Technology as one of the projects of the Differential Equations Group in the Center for Research on Parallel Computation. In what follows, we describe the interface FORTRAN code for AUTO to simulate the laser diodes with external cavity and some representative results. We stress that the results shown here only apply to the particular parameters chosen as indicated. To find the dynamic behavior of ECLDs with different parameters, one needs to run the AUTO program with the interface FORTRAN code with the modified ECLD parameters.

3.1 Bifurcation Diagrams of ECLD Steady States

To construct the bifurcation diagrams of ECLD steady states, the first step is to find all ECLD steady states for a given set of the ECLD parameters and then using AUTO to finding the continuations of the steady states.

To find all ECLD steady states for a given set of the ECLD parameters, one needs to find all the solutions to the nonlinear algebraic equations:

$$(g-\frac{1}{\tau_p})S(t)+2\kappa\sqrt{S(t)}\sqrt{S(t-\tau)}\cos(\Omega_s\tau+\phi(t)-\phi(t-\tau))=0 \quad (6)$$

$$J-\frac{N(t)}{\tau_{sp}}-gS(t)=0 \quad (7)$$

arrived by setting the right-hand side of Eqs. (3) and (5) to be equal to zero.

Once all the steady states of the ECLD for the given set of parameters are found, the bifurcation diagram can be constructed by continuing the steady states as one of the parameters in the parameter set is varied in both directions (increasing or decreasing). It is found that Hopf bifurcation delineates stable and unstable steady states.

3.2 Stability Boundaries of ECLD Modes

To construct the Stability-Boundary diagram of ECLD steady states, the first step is to find the Hopf bifurcation points of all ECLD steady states for a given set of the ECLD parameters and then using AUTO to finding the continuations of the Hopf bifurcation points.

To find Hopf bifurcation points of all ECLD steady states for a given set of the ECLD parameters, one needs to find all the solutions to the nonlinear algebraic equations (6), (7), and (8)

$$\begin{aligned}D(s) &= -s^3+s^2\left[\gamma+2\kappa e(\tau)\cos\phi\right]-s\left[\omega_R{}^2+\kappa^2e^2(\tau)+2\gamma_e\kappa e(\tau)\cos\phi\right]\\ &+\kappa\left[\omega_R{}^2e(\tau)(\cos\phi-\alpha\sin\phi)+\gamma_e\kappa e^2(\tau)+\alpha\gamma_e\gamma_p e(\tau)\sin\phi\right]\end{aligned} \quad (8)$$

where $e(\tau) = 1 - e^{i\omega\tau}$ and $\phi = \Omega\tau$. Here $\gamma_e = 1/\tau_s + g_N S$ is the carrier perturbation decay rate, $\gamma = \gamma_e + \gamma_p$ is the decay rate of relaxation oscillations, with $\gamma_p = g\kappa_p P$ being the contribution of the nonlinear gain. The angular frequency of relaxation oscillations ω_R is given by $\omega_R^{\,2} = gg_N S + \gamma_e\gamma_p$. Equation (8) is arrived by setting the determinant of the linearized ECLD system to be equal to zero.

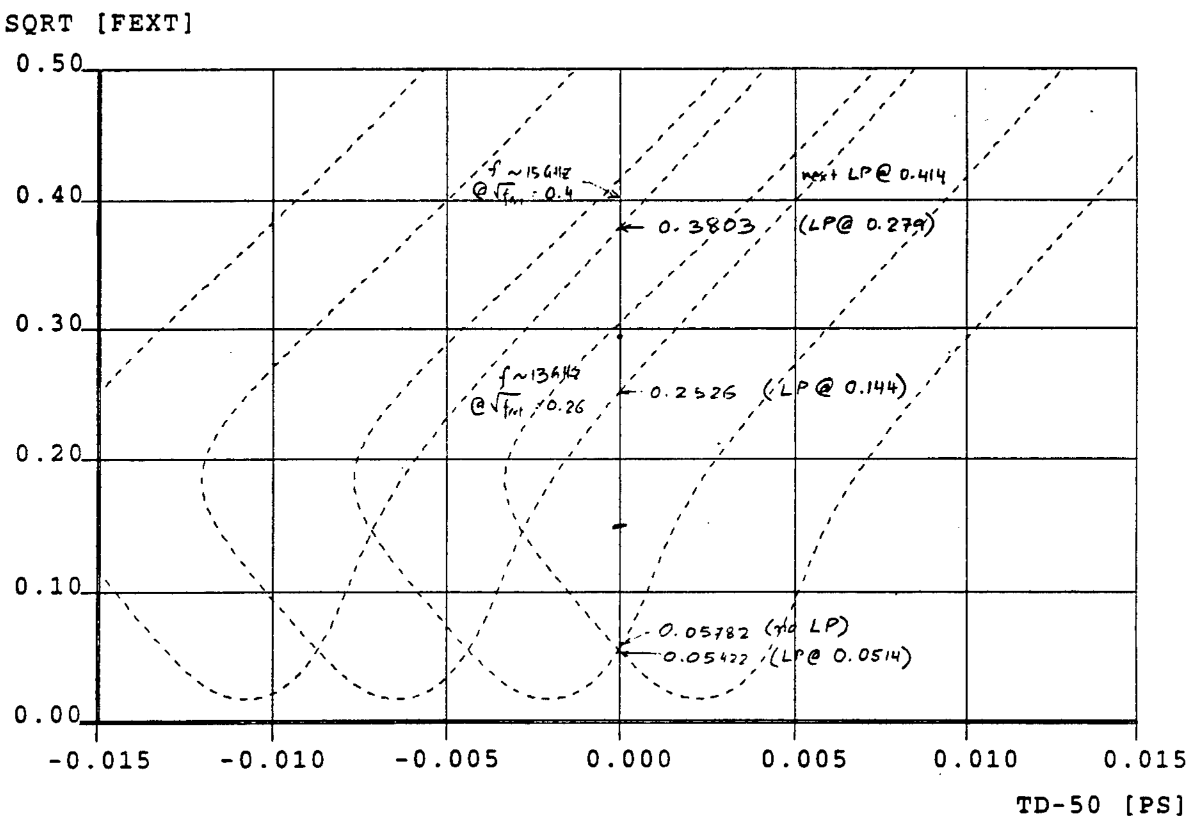

Fig. 3 The stability boundaries of 4 ECLD modes in the $\sqrt{f_{ext}} - \tau_d$ plane. The injection current is at twice the threshold. The meaning of LP is explained subsequently.

Once Hopf bifurcation points of all the steady states of the ECLD for the given set of parameters are found, the bifurcation diagram can be constructed by continuing the steady states when one of the parameters in the parameter set is varied in both directions (increasing or decreasing). An example is shown in Fig. 3.

3.3 Regions of Existence of ECLD Modes

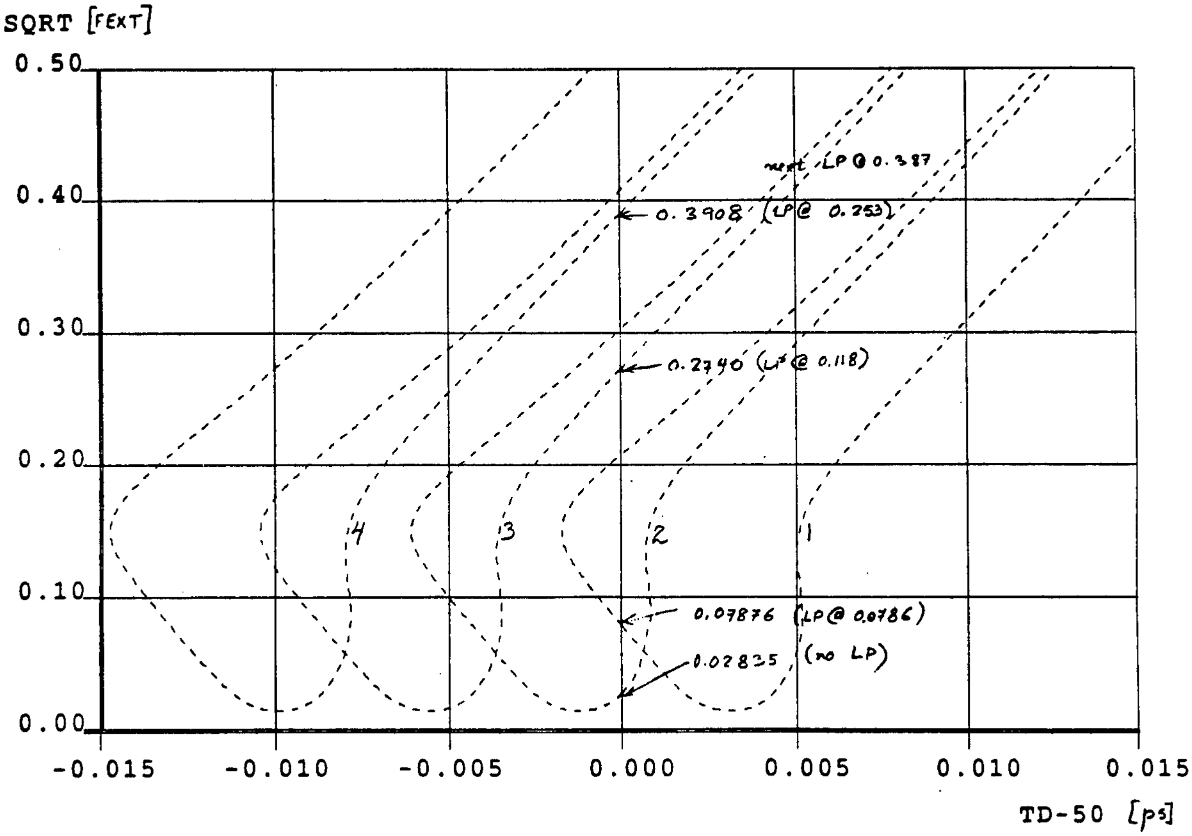

Fig. 4 Limiting points (LP) of existence of modes superimposed on the stability boundaries. When LP of a higher-order mode is above the stability boundary, robust high-frequency oscillations result. Parameter same as in Fig. 3, except that injection is three times the threshold.

It is found by numerical simulation that even in regions above the stability boundary of a particular, the high-frequency oscillations are not always present. We believe that this due to the existence of other modes, which might be stable in the unstable region of the mode that we are interested in. To do so, we calculated the regions of existence of all modes. High-frequency oscillations are produced only if the boundary of existence [limiting point (LP) of existence] of higher-order modes is above the stability boundary. An example where robust high-frequency oscillations are possible is shown in Fig. 4. A careful examination of Fig. 3 reveals that robust high-frequency oscillations are not possible, even though the bifurcation analysis alone predicts the existence of the high-frequency oscillations.

3.4 Experimental Generation of High-Frequency Oscillation

Using a Fabry-Perot laser diode and an optical flat as the external mirror, The high-frequency intensity oscillations have been generated in Rome Lab by Steve Johns. The highest frequency achieved is 9.5 GHz. Modulation of these oscillations has also been demonstrated. Up to 750 MHz modulation has shown excellent frequency modulation characteristics with minimal residual amplitude modulation.

4. Investigation of the Noise Characteristics

4.1 Preliminary Comment

Periodic orbits in nonlinear optical systems, such as the high-frequency oscillations described in Sections 2 and 3 can serve as subcarriers in optical communications. Subcarrier optical communication using one form of periodic orbits commonly known as self-sustained pulsations (SSP) [5] has been experimentally demonstrated both for analog [6] and digital [7] applications. The signal-to-noise ratio (bit-error-rate) of the analog (digital) subcarrier systems depends on the nature and magnitude of the noise of the subcarrier. Since only one harmonic in SSP is used as the subcarrier, the amplitude and phase noise of each harmonic in SSP needs to be characterized. In this repoty we report the first, to the best of our knowledge, calibrated measurement of amplitude and phase noise of self-pulsations in two-section Fabry-Perot laser diodes (LDs).

4.2 Experimental Setup

Figure 1 illustrates the experimental setup for the measurement of amplitude and phase noise of SSP in commercially available 780 nm SSP LDs. The SSP is first converted into RF signals with a high-speed photodetector (3 dB bandwidth >14 GHz). The RF spectrum of SSP is monitored using a broadband RF spectrum analyzer (HP 8565E). By using bandpass filters, individual harmonic of the RF signal can be selected for amplitude and phase noise measurement using the HP 3048A Noise Measurement

System, which is a calibrated measurement system dedicated for RF/microwave oscillator noise characterization for frequency offsets as small as 1 Hz.

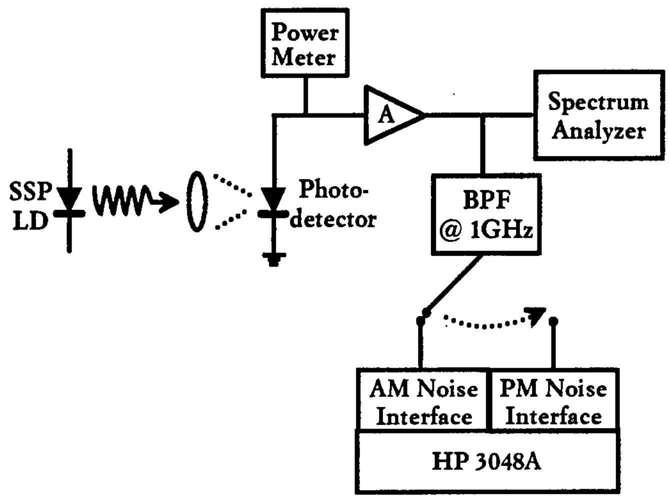

Figure. 5 Experimental setup for the amplitude and phase noise measurement

4.3 Results

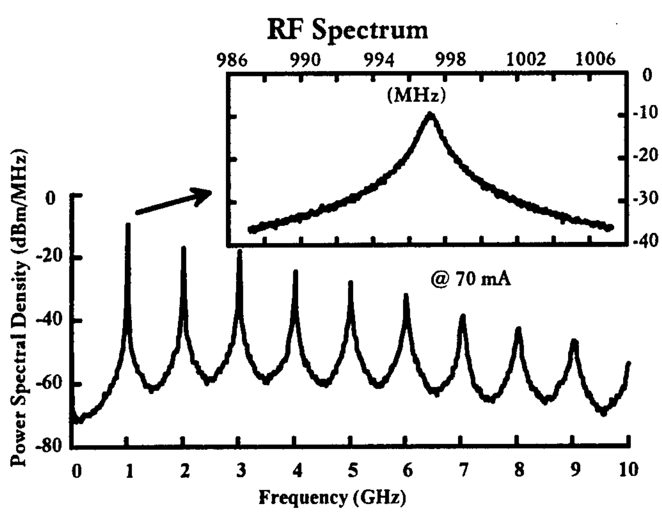

Figure. 6 RF spectrum of SSP with a 1 GHz fundamental frequency in a laser diode.

A typical RF spectrum of SSP is shown in figure 2. At 70 mA DC bias current, the SSP frequency is around 1 GHz (The threshold is at 50 mA). More than 15 harmonics can be observed. Each harmonic has a certain linewidth which increases with its order. Details around the fundamental harmonic, given in the inset, reveals a 3-dB linewidth on the order of 1 MHz. Because the fundamental harmonic was used in previous experiments [6,7] and because of the instrumentation frequency limitations, we focused on the noise characterization of the fundamental harmonic in the present effort. With a 1 GHz bandpass filter of 400 MHz bandwidth, the amplitude and phase noise of fundamental harmonic are investigated nearly independent of each.

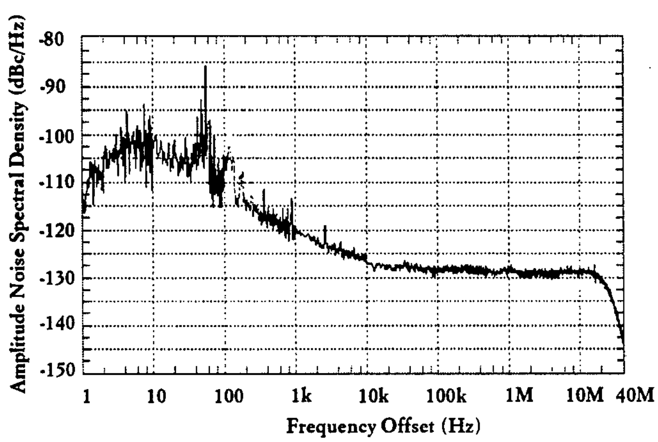

Figure. 7 Amplitude noise spectrum of the fundamental harmonic.

The amplitude noise is measured first because the AM noise interface offers a better than 110-dB discrimination against phase noise. The amplitude noise spectral density in dBc, which represents the AM noise sideband to carrier power ratio, is given in figure 3. Comparing the RF and AM noise spectra, it is apparent that amplitude noise has a negligible contribution to the overall noise power leading to the 1 MHz linewidth. Therefore, the noise of the fundamental harmonic has to be primarily phase noise. The phase noise interface is essentially a delay-line frequency discriminator which measures the noise frequency deviation from the center frequency due to phase noise. Figure 4 shows the phase noise spectrum of the fundamental harmonic for 1 Hz to 40 MHz frequency offset from the center frequency of the carrier. Below 1 kHz offset, the noise frequency deviation is 1/f in nature. The peak around 60 Hz results from the power supply. For the frequency offsets above 10 kHz, frequency deviation noise is white with a magnitude of around $600\,Hz/\sqrt{Hz}$. The decrease near 40 MHz offsets is due to the bandwidth limitation of the HP 3048A system. Assuming a $600\,Hz/\sqrt{Hz}$ pure frequency fluctuation which is white in nature, the theoretically [8] estimated carrier linewidth is about 1.13 MHz which matches very well with the observed RF spectrum.

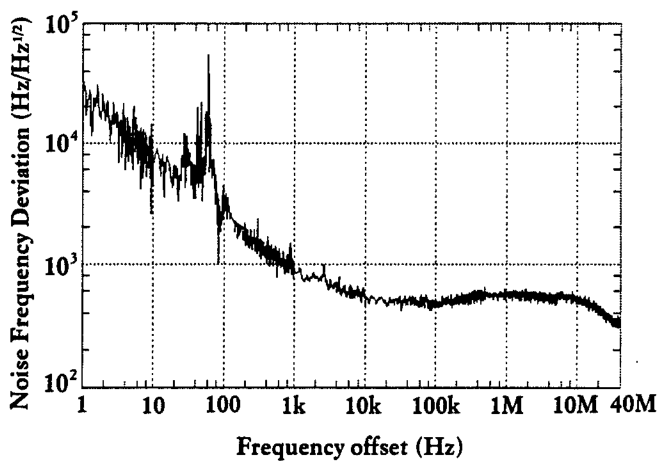

Figure. 4 Phase noise spectrum of the fundamental harmonic

4.4 Summary

We have investigated experimentally the noise behavior of self-sustained pulsation in laser diodes. Frequency deviation and amplitude fluctuation of the pulsation have been characterized in the range of 1 Hz to 40 MHz. Even though phase noise dominates over amplitude noise, both are 1/f in nature for offsets below 1 kHz, and white for offsets above 10 kHz. This technique can be applied to the noise measurement of the high-frequency oscillation in ECLDs also.. In addition to understanding and ultimately improving the performance of periodic-orbit subcarrier optical communication systems, further research along this line will be useful for other applications such as all-optical clock recovery [9].

5. Conclusions

In conclusion, we have determine the underlying mechanism of the high-frequency intensity oscillations in laser diodes with short external cavity. From a nonlinear dynamic point of view, Hopf bifurcation is responsible for the occurrence of the high-frequency intensity oscillations. However, Hopf bifurcation is only the necessary condition. The necessary and sufficient condition are that Hopf bifurcation occurs and the limiting point of existence of a higher-order mode is above the stability boundary of a lower-order mode. The noise characteristics of the high-frequency oscillations can be measured using the HP 3048A phase and amplitude noise measurement system.

References

1. BJARNE TROMBORG and JESPER MORK, "Nonlinear injection locking dynamics and the onset of coherence collapse in external cavity lasers," IEEE J. Quantum Electron. , vol. QE-26, pp.642-654, Apr.1990
2. J. Mork , B. Tromborg , and J. Mark , " Chaos in semiconductor lasers with optical feedback : Theory and experiments," IEEE J. Quantum Electron. , vol. 28, pp. 93-108, Jan. 1992.
3. William H. Press, Brian P. Flannery, Saul A. Teukolsky and William T. Vetterling, Numerical Recipes : The art of scientific computing . Cambridge University Press 1986 .
4. David Kincaid and Ward Cheney, Numerical Analysis . Brooks/Cole Publishing company, Pacific Grove, California, 1991 .
5. T.L. Paoli and J. Ripper, "Optical pulses from cw GaAs injection laser," Appl. Phys. Lett. 15, 1965, pp.105-107.
6. X. Wang, G. Li and C. S. Ih, "Microwave/millimeter-wave frequency subcarrier lightwave modulations based on self-sustained pulsation of laser diode," J. Lightwave Technol., 1993, pp. 309-314.
7. J. B. Geroges and K. Y. Lau, "Self-pulsating laser diodes as fast-tunable ($\leq$ 1ns) FSK transmitters in subcarrier multiple-access networks," IEEE Photonics Technol. Lett., 1993, pp 242-245.
8. T. Okoshi and K. Kikuchi, *Coherent Optical Fiber Communications*, Kluwer Academic Publishers, Boston, 1988.
9. U. Feister, D. J. As and A. Ehrhardt, "18 GHz all-optical frequency locking and clock recovery using a self-pulsating two-section DFB-laser," IEEE Photonics Technol. Lett., 1994, pp 106-108.

☆U.S. GOVERNMENT PRINTING OFFICE: 1997-610-130-61082

MISSION OF ROME LABORATORY

Mission. The mission of Rome Laboratory is to advance the science and technologies of command, control, communications and intelligence and to transition them into systems to meet customer needs. To achieve this, Rome Lab:

a. Conducts vigorous research, development and test programs in all applicable technologies;

b. Transitions technology to current and future systems to improve operational capability, readiness, and supportability;

c. Provides a full range of technical support to Air Force Material Command product centers and other Air Force organizations;

d. Promotes transfer of technology to the private sector;

e. Maintains leading edge technological expertise in the areas of surveillance, communications, command and control, intelligence, reliability science, electro-magnetic technology, photonics, signal processing, and computational science.

The thrust areas of technical competence include: Surveillance, Communications, Command and Control, Intelligence, Signal Processing, Computer Science and Technology, Electromagnetic Technology, Photonics and Reliability Sciences.